

1 **Supplementary Data S1. Materials and methods**

2 **Transcriptomic analysis**

3 Total RNA was extracted with Trizol™ X-100 (Thermo Fisher Scientific, USA) and a total amount
4 of 2 µg RNA per sample was used as input material for the RNA sample preparations. Sequencing
5 libraries were generated using VAHTS mRNA-seq v2 Library Prep Kit (Illumina, USA). mRNA was
6 purified from total RNA using poly-T oligo-attached magnetic beads and cut into small fragments for
7 cDNA synthesis. After adenylation of 3' ends of DNA fragments, adaptors with hairpin loop structure
8 were ligated, and then PCR was performed. High-throughput RNA sequencing was carried out using the
9 Illumina NovaSeq platform. Raw data were filtered and processed by Q30 and aligned to the mouse
10 reference genome GRCm38/mm10 with Hisat2 software. Quantification of the transcripts was
11 accomplished with featureCounts software guided by the Ensembl gtf gene annotation file
12 (<http://www.ensembl.org/>). Fragments Per Kilobase of transcript per Million mapped reads (FPKM) were
13 used for the measurements of the relative abundances of the transcripts. An effective expressed gene
14 required an FPKM score greater than one.

15 **Proteomic analysis**

16 Heart tissues were subjected to protein extraction, digestion and Tandem Mass Tags (TMT) labeling.
17 In brief, tissues were disrupted by tissuelyser and lysed with protein extraction buffer [8 M urea, 75 mM
18 NaCl, 50 mM Tris, pH 8.2, 1% (vol/vol) EDTA-free protease inhibitor, 1 mM NaF, 1 mM β-
19 glycerophosphate, 1 mM sodium orthovanadate, 10 mM sodium pyrophosphate] (Sigma-Aldrich, USA)
20 followed by centrifugation. Protein concentrations were determined using Bradford assay (Beyotime,
21 China). Cysteine residues were reduced with 5 mM DTT (Thermo Fisher Scientific, USA) for 25 min at
22 56 °C followed by alkylation with 14 mM iodoacetamide (Sigma-Aldrich, USA) for 30 min in dark, and
23 unreacted iodoacetamide was quenched by DTT for 15 min. The urea concentration was diluted with 25
24 mM Tris (Sigma-Aldrich, pH 8.2, USA) to 1.2 M, and the proteins were digested overnight at 37°C with
25 5 ng/µL trypsin (Promega, USA, USA) and 1 mM CaCl₂ (Sigma-Aldrich, USA). The peptides were
26 desalted by tC18 Sep-Pak column (Waters), followed by TMT 10-Plex (Thermo Fisher Scientific, USA)
27 labeling. After labeling, each of the 3 groups was mixed respectively and desalted by Waters tC18 Sep-
28 Pak column.

29 For protein quantification, 40 µg TMT-labeled peptide mixture was fractionated using ACQUITY
30 UPLC M-Class with XBridge BEH C18 column (300 µm×150 mm, 1.7µm; 130Å, Waters). 25 fractions
31 were collected by using nonadjacent pooling scheme within a 128 min gradient of 3% buffer B (A: 10
32 mM ammonium formate, pH 10; B: 100% acetonitrile) for 14 min, 3%–8% buffer B for 1 min, 8%–29%
33 buffer B for 71 min, 29%–41% buffer B for 12 min, 41%–100% buffer B for 1 min, 100% buffer B for
34 8 min, 100%–3% buffer B for 1 min followed by 20 min in 3% buffer B.

35 For liquid chromatography-tandem mass spectrometry (LC-MS) analyses, TMT-labeled peptides were
36 resuspended in 0.1% formic acid and analyzed using an LTQ Orbitrap Fusion Lumos mass spectrometer
37 (Thermo Finnigan, USA) coupled to the Easy-nLC 1200. The trap column (75µm×2cm, Acclaim®
38 PepMap100 C18 column, 3µm, 100 Å; DIONEX, Sunnyvale, CA) effluent was transferred to a reverse-
39 phase microcapillary column (75µm×25cm, Acclaim® PepMap RSLC C18 column, 2µm, 100 Å;
40 DIONEX, Sunnyvale, CA). For protein quantification analysis, a 95 min linear gradient (3% to 5% buffer
41 B for 5 s, 5% to 15% buffer B for 40 min, 15% to 28% buffer B for 34.8 min, 28% to 38% buffer B for
42 12 min, 30% to 100% buffer B for 5 s and 100% buffer B for 8 min) was applied while using the following
43 buffer: 0.1% formic acid (buffer A) and 80% acetonitrile, 0.1% formic acid (buffer B). The Orbitrap

44 Fusion Lumos mass spectrometer was operated in the data-dependent mode. A full survey scan was
45 obtained for the m/z range of 350–1,500, and the resolution of higher-energy collision dissociation
46 tandem mass spectrometry (HCD MS/MS) was 50,000.

47 MS raw files (.raw) were searched against the mouse protein sequences obtained from the Universal
48 Protein Resource Database (UniProt, downloaded in July 18, 2018 containing 76,117 sequences) by
49 MaxQuant software [27809316] (version 1.6.5.0) for feature detection, database searching, and protein
50 quantification. N-terminal protein acetylation and methionine oxidation were set as variable
51 modifications, and carbamidomethylation of cysteine residues was set as a fixed modification. The
52 minimum peptide length was 6 amino acids, and the maximum missed cleavage for each peptide was 2.
53 False discovery rates (FDR) cut-offs were set to 0.01 for both proteins and peptides. All other parameters
54 were the default settings of the MaxQuant software.

55 **Metabolomics analysis**

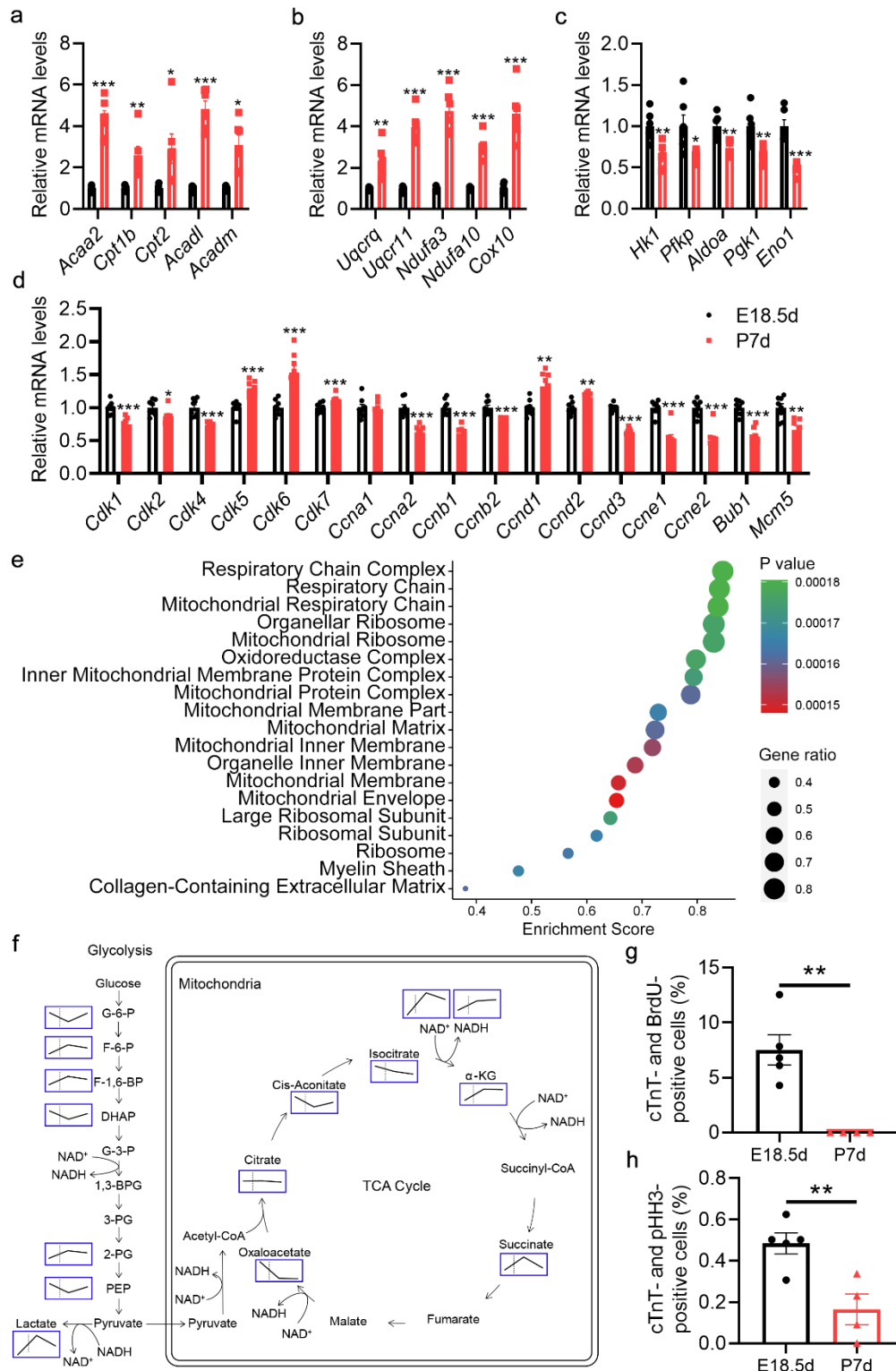
56 For metabolome analysis, the heart samples were mixed and freeze-dried as required. Then the
57 sample was weighted to an EP tube, and extract solution (acetonitrile: methanol: water = 2: 2: 1)
58 containing internal standard (L-2-Chlorophenylalanine, 2 µg/mL) was added. After 30 s vortex, the
59 samples were homogenized at 35 Hz for 4 min and sonicated for 5 min in an ice-water bath. The
60 homogenization and sonication cycle were repeated 3 times. Then the samples were incubated at -40°C
61 for 1 h and centrifuged at 10,000×rpm for 15 min at 4°C. 400 µL of supernatant was transferred to a fresh
62 tube and dried in a vacuum concentrator at 37°C. Then, the dried samples were reconstituted in 200 µL
63 of 50% acetonitrile by sonication on ice for 10 min. The constitution was then centrifuged at 13,000×rpm
64 for 15 min at 4°C, and 75 µL of supernatant was transferred to a fresh glass vial for LC/MS analysis. The
65 quality control sample was prepared by mixing an equal aliquot of the supernatants from all the samples.

66 The ultra-high-pressure liquid chromatography (UHPLC) separation was carried out using a 1290
67 Infinity series UHPLC System (Agilent Technologies, USA), equipped with a UPLC BEH Amide
68 column. The mobile phase consisted of 25 mM ammonium acetate and 25 mM ammonia hydroxide in
69 water (pH = 9.75) (A) and acetonitrile (B). The analysis was carried with elution gradient as follows:
70 0~0.5 min, 95% B; 0.5~7.0 min, 95%~65% B; 7.0~8.0 min, 65%~40% B; 8.0~9.0 min, 40% B; 9.0~9.1
71 min, 40%~95% B; 9.1~12.0 min, 95% B. The column temperature was 25°C. The auto-sampler
72 temperature was 4°C, and the injection volume was 2 µL (positive) or 2 µL (negative), respectively.

73 The TripleTOF 6600 mass spectrometry (AB Sciex) was used for its ability to acquire MS/MS
74 spectra on an information-dependent basis (IDA) during an LC/MS experiment. In this mode, the
75 acquisition software (Analyst TF 1.7, AB Sciex) continuously evaluates the full scan survey MS data as
76 it collects and triggers the acquisition of MS/MS spectra depending on preselected criteria. In each cycle,
77 the most intensive 12 precursor ions with intensity above 100 were chosen for MS/MS at collision energy
78 (CE) of 30 eV. The cycle time was 0.56 s. ESI source conditions were set as follows: Gas 1 as 60 psi,
79 Gas 2 as 60 psi, Curtain Gas as 35 psi, Source Temperature as 600°C, Declustering potential as 60 V, Ion
80 Spray Voltage Floating (ISVF) as 5000 V or -4000 V in positive or negative modes, respectively.

81 MS raw data (.wiff) files were converted to the mzXML format by ProteoWizard, and processed by
82 R package XCMS (version 3.2). The process includes peak deconvolution, alignment and integration.
83 Minfrac and cut off were set as 0.5 and 0.3 respectively. An in-house MS2 database was applied for
84 metabolite identification.

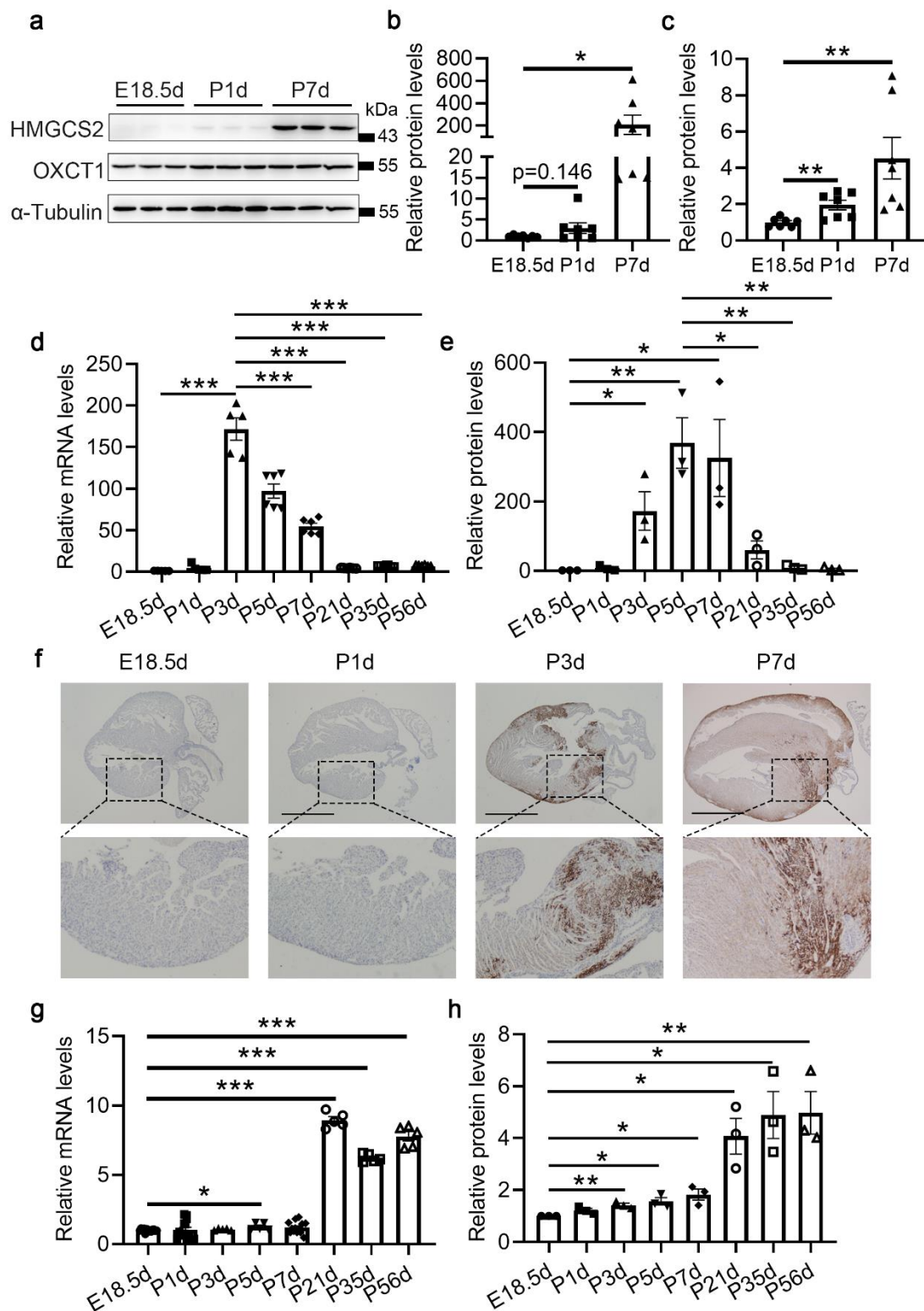
85



86

87 **Fig. S1 Metabolic reprogramming and cell cycle arrest take place in the neonatal mouse**
 88 **heart. a-d** qPCR detection of the mRNA levels of genes related to FA beta oxidation (a, $n = 6$ for each
 89 group), mitochondrial oxidative phosphorylation (b, $n = 6$ for each group), glycolysis (c, $n = 6$ for each
 90 group) and cell cycle (d, $n = 8$ for each group) in the hearts of E18.5d and P7d mice. **e** GSEA of the
 91 proteins in perinatal mouse hearts (P7d vs E18.5d) according to Gene Ontology (GO) cellular component
 92 (cc) terms. **f** Metabolome analysis of the glycolytic pathway and the TCA cycle in perinatal mouse hearts

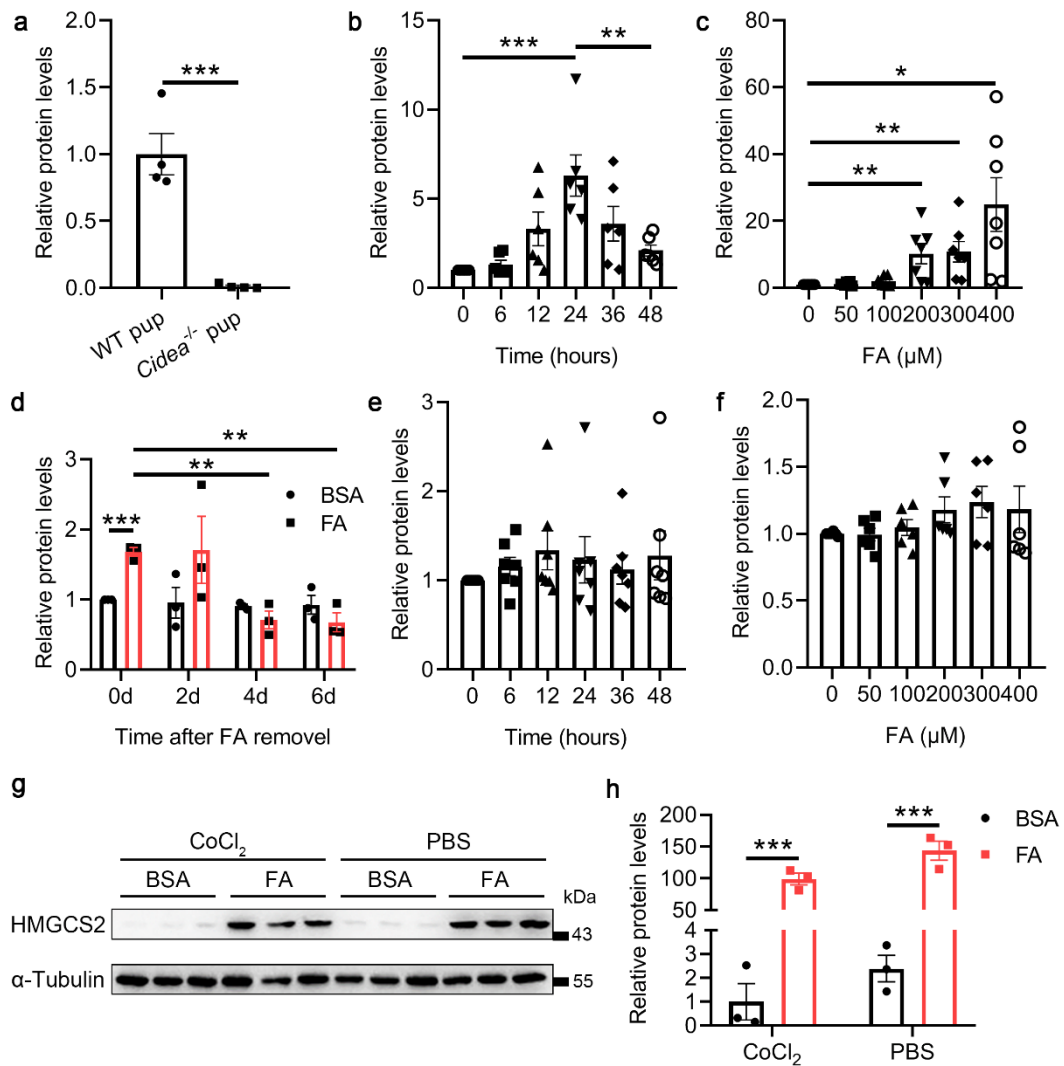
93 (E18.5d, P1d, and P7d). The dotted line represents the point of birth. **g** The statistics of the percentages
94 of cTnT and BrdU double-positive cells in Fig. 1i ($n = 4-5$ for each group). **h** The statistics of the
95 percentages of cTnT and pHH3 double-positive cells in Fig. 1j ($n = 4-5$ for each group). Data are
96 presented as mean \pm SEM. and the P values were determined by unpaired two-tailed Student's t -test. *,
97 $P < 0.05$; **, $P < 0.01$; ***, $P < 0.001$.



98

99 **Fig. S2 Enhanced ketogenesis occurs in neonatal mouse heart.** **a** Western blot detection of
 100 the protein levels of HMGCS2 and OXCT1 in E18.5d, P1d and P7d mouse hearts. **b** Quantitative analysis
 101 of the HMGCS2 protein levels in heart tissues in Fig. S2a ($n = 7$ for each group). **c** Quantitative analysis
 102 of the OXCT1 protein levels in heart tissues in Fig. S2a ($n = 7$ for each group). **d** qPCR detection of
 103 *Hmgcs2* mRNA levels in mouse hearts from the embryonic period to adulthood ($n = 5-6$ for each group).

104 **e** Quantitative analysis of the HMGCS2 protein levels in heart tissues in Fig. 2e ($n = 3$ for each group).
105 **f** Immunohistochemical analysis of HMGCS2 expression in the mouse hearts. Scale bar, 2 mm. **g** qPCR
106 detection of *Oxct1* mRNA levels in mouse hearts from the embryonic period to adulthood ($n = 5-13$ for
107 each group). **h** Quantitative analysis of the OXCT1 protein levels in Fig. 2h ($n = 3$ for each group). Data
108 are presented as mean \pm SEM. and the P values were determined by one-way ANOVA. *, $P < 0.05$; **,
109 $P < 0.01$; ***, $P < 0.001$.



110

111 **Fig. S3 Colostrum FA promotes transient massive expression of *Hmgcs2* in neonatal**
 112 **mouse heart.** **a** Quantitative analysis of the HMGCS2 protein levels in Fig. 3a ($n = 4$ for each group).
 113 **b** Quantitative analysis of the HMGCS2 protein levels in Fig. 3c ($n = 6$ for each group). **c** Quantitative
 114 analysis of the HMGCS2 protein levels in Fig. 3e ($n = 7$ for each group). **d** Quantitative analysis of the
 115 HMGCS2 protein levels in Fig. 3f ($n = 3$ for each group). **e** Quantitative analysis of the OXCT1 protein
 116 levels in Fig. 3h ($n = 7$ for each group). **f** Quantitative analysis of the OXCT1 protein levels in Fig. 3j (n
 117 = 6 for each group). **g** NRVMs were treated with FA (200 μM) and CoCl₂ (100 μM) separately or at the
 118 same time for 24 h, and then western blotting was performed to detect the protein level of HMGCS2. **h**
 119 Quantitative analysis of the HMGCS2 protein levels in Fig. S3g ($n = 3$ for each group). Data are presented
 120 as mean ± SEM, and the P values were determined by one-way ANOVA and unpaired two-tailed
 121 Student's t -test. *, $P < 0.05$; **, $P < 0.01$; ***, $P < 0.001$.

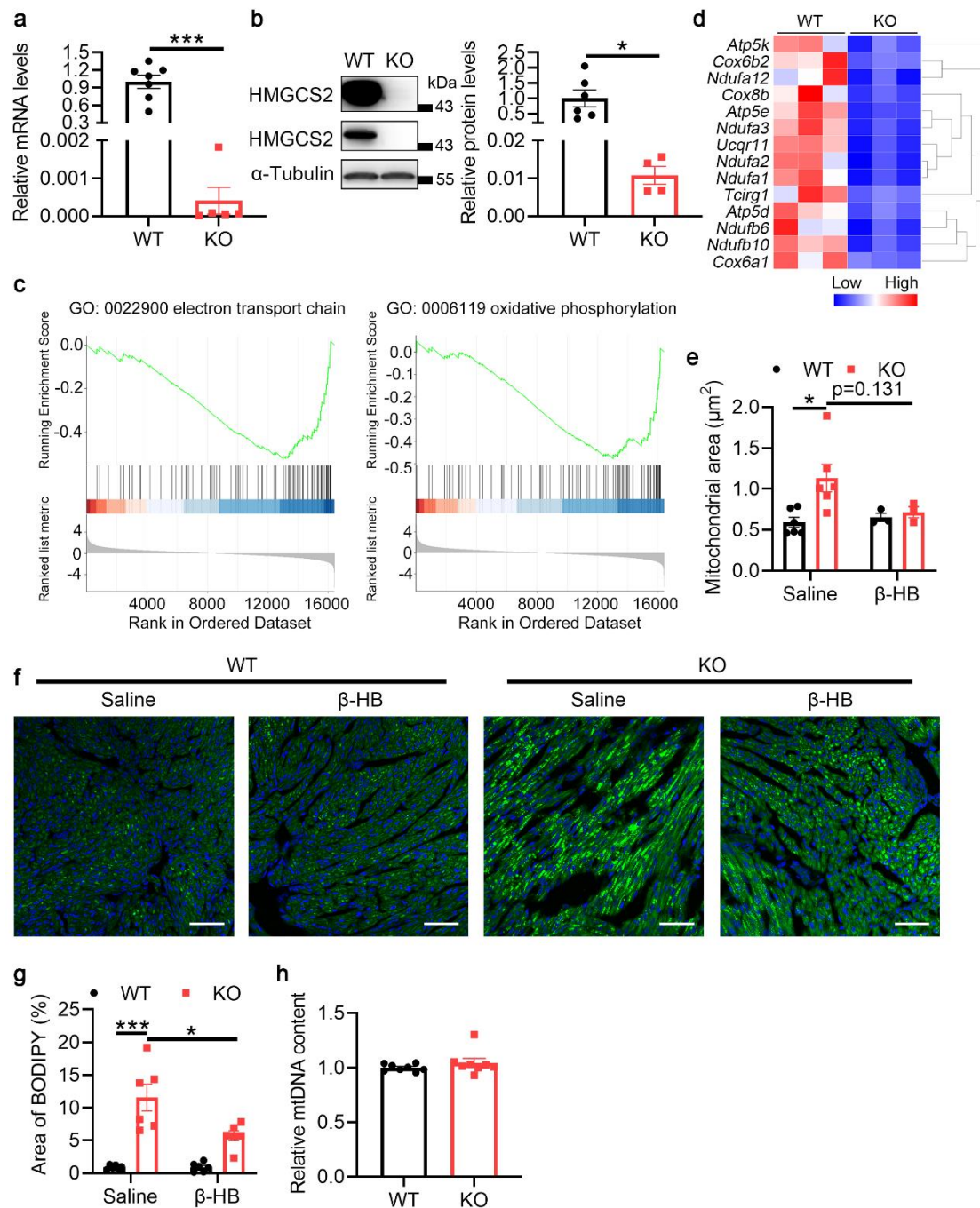


Fig. S4 Ketone body deficiency causes mitochondrial maturation disorder in neonatal

mouse heart. **a, b** Detection of the mRNA (a) and protein levels (b) of *Hmgcs2* in the hearts of P5d

WT and KO mice. **c** Transcriptomics GSEA score curves: the alteration of mRNA levels related to

electron transport chain (left) and oxidative phosphorylation (right) in P3d KO hearts compared with that

in WT hearts. **d** Heatmap of mRNA levels related to electron transport chain and oxidative

phosphorylation in P3d WT hearts and KO hearts. **e** Statistical analysis of the area of a single

mitochondrion in Fig. 4d ($n = 3-6$ for each group). **f** BODIPY staining in the hearts of P5d WT and KO

mice treated with saline or β -HB (400 mg/kg/day though i.p. from P3d to P5d). Scale bar, 50 μm . **g**

Statistical analysis of the area of BODIPY in Fig. S4f ($n = 6$ for each group). **h** qPCR detection of the

mtDNA levels (*mt-Co1*, *mt-Dloop*, *mt-Atp6*) in the hearts of P5d WT and KO mice ($n = 8$ for each group).

Data are presented as mean \pm SEM. and the P values were determined by unpaired two-tailed Student's

122

123

124

125

126

127

128

129

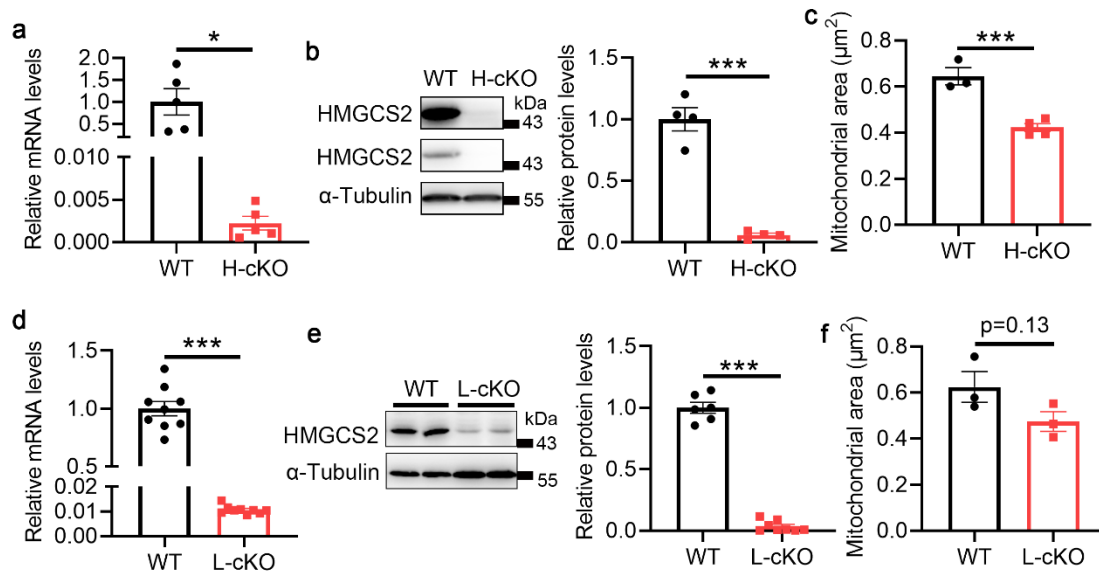
130

131

132

133

134 *t*-test. *, $P < 0.05$; ***, $P < 0.001$.

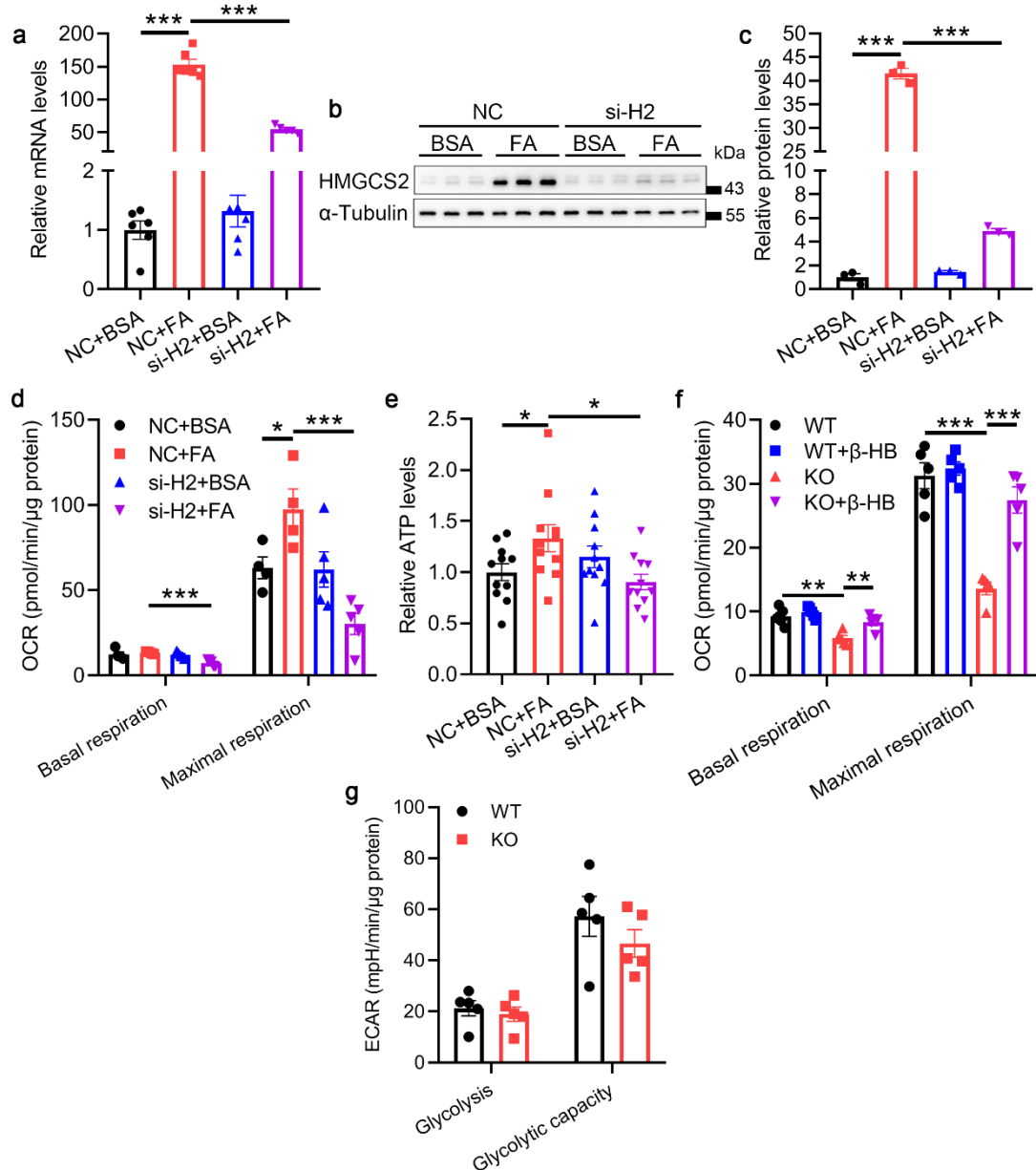


135

136 **Fig. S5 Heart and liver-specific knockout of *Hmgcs2* has no effect on mitochondrial**
137 **maturation in neonatal mouse hearts. a, b** Detection of the mRNA ($n = 5$ for each group, a) and
138 protein levels ($n = 4$ for each group, b) of *Hmgcs2* in the hearts of P5d WT and H-cKO mice. c Statistical
139 analysis of the area of a single mitochondrion in Fig. 4i (WT, $n = 3$; H-cKO, $n = 4$). d, e Detection of the
140 mRNA ($n = 9$ for each group, d) and protein levels ($n = 6-8$ for each group, e) of *Hmgcs2* in the livers of
141 P5d WT and L-cKO mice. f Statistical analysis of the area of a single mitochondrion in Fig. 4l ($n = 3$ for
142 each group). Data are presented as mean \pm SEM. and the P values were determined by unpaired two-
143 tailed Student's *t*-test. *, $P < 0.05$; ***, $P < 0.001$.

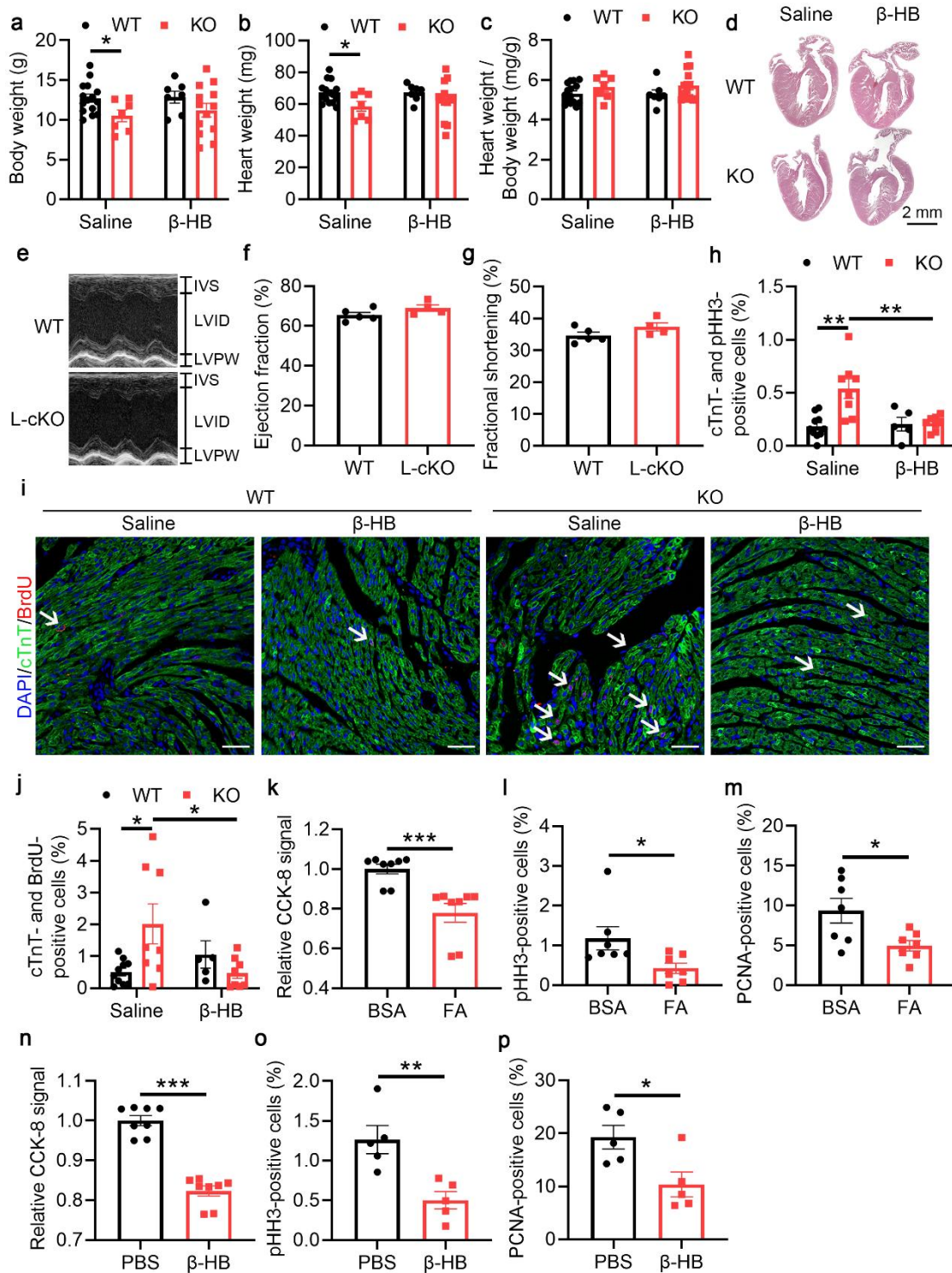
144

145



146

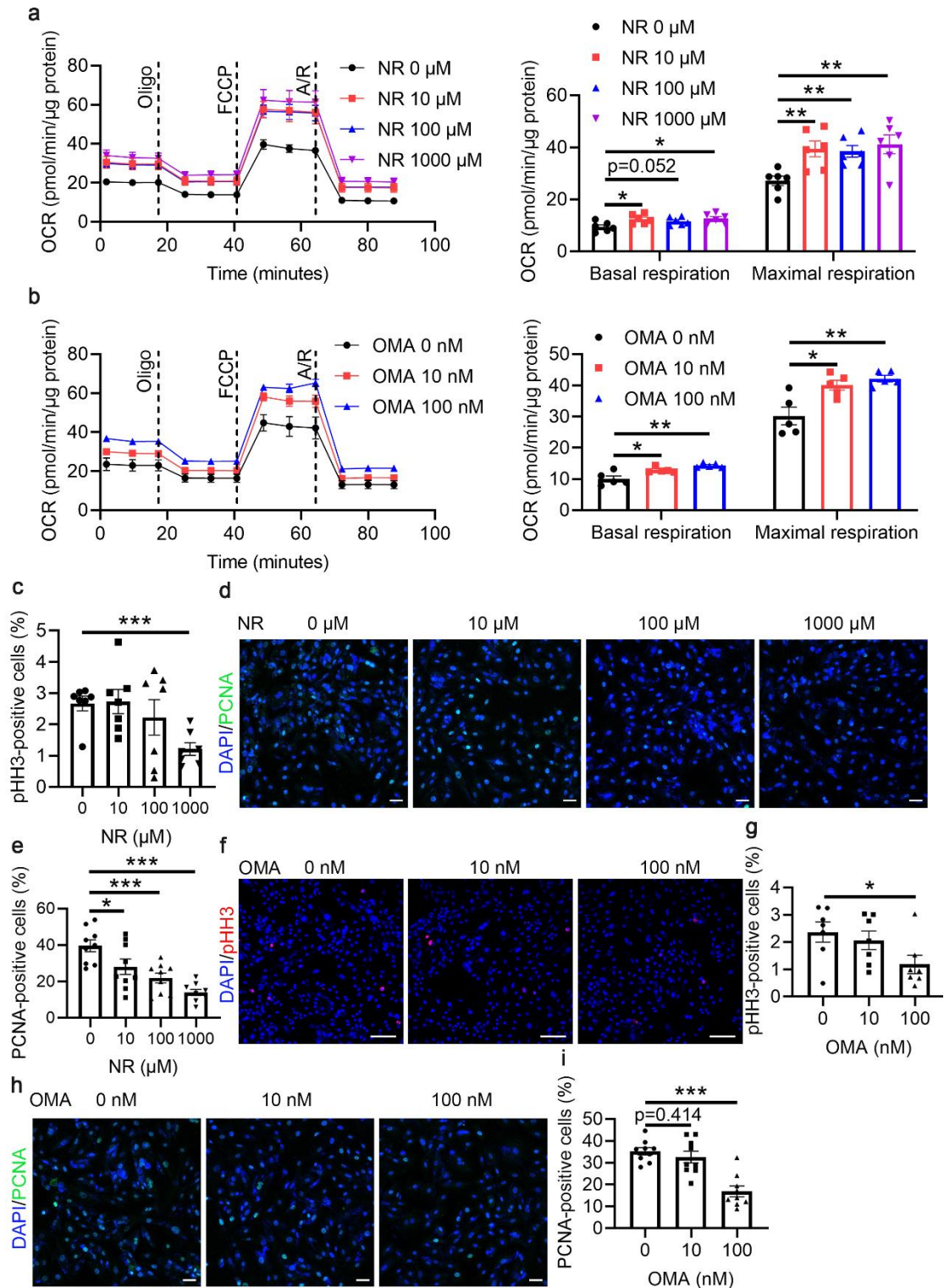
147 **Fig. S6 *Hmgcs2* and ketone body β -HB regulate FA-stimulated mitochondrial oxidative**
 148 **metabolism without affecting glycolysis in neonatal mouse heart.** **a** qPCR detection of
 149 *Hmgcs2* mRNA levels in negative control and *Hmgcs2*-silenced NRVMs treated with BSA or 200 μ M
 150 FA ($n = 5-6$ for each group). **b** Western blot detection of HMGCS2 protein levels in negative control and
 151 *Hmgcs2*-silenced NRVMs treated with BSA or 200 μ M FA. **c** Quantitative analysis of the HMGCS2
 152 protein levels in Fig. S6b ($n = 3$ for each group). **d** Statistical analysis of the basal respiration and maximal
 153 respiration capacity in Fig. 5c ($n = 4-5$ for each group). **e** Relative ATP levels in negative control and
 154 *Hmgcs2*-silenced NRVMs treated with BSA or 200 μ M FA ($n = 11$ for each group). **f** Statistical analysis
 155 of the basal respiration and maximal respiration capacity in Fig. 5d ($n = 5$ for each group). **g** Statistical
 156 analysis of the basal glycolysis and maximal glycolytic capacity in Fig. 5e ($n = 5$ for each group). Data
 157 are presented as mean \pm SEM, and the P values were determined by unpaired two-tailed Student's t -test.
 158 *, $P < 0.05$; ***, $P < 0.001$.



160

161 **Fig. S7 Neonatal ketone body elevation is essential for postnatal heart development and**
 162 **heart function.** **a** Body weights of WT and KO mice at P21d (WT+Saline, $n = 15$; KO+Saline, $n = 7$;
 163 WT+ β -HB, $n = 7$; KO+ β -HB, $n = 13$). **b** Heart weights of WT and KO mice at P21d (WT+Saline, $n =$
 164 15 ; KO+Saline, $n = 7$; WT+ β -HB, $n = 7$; KO+ β -HB, $n = 13$). **c** Heart weight/body weight ratios of WT
 165 and KO mice at P21d (WT+Saline, $n = 15$; KO+Saline, $n = 7$; WT+ β -HB, $n = 7$; KO+ β -HB, $n = 13$). **d**
 166 Representative longitudinal sections after H&E staining of WT and KO mouse hearts at P21d. Scale bar,
 167 2 mm. **e** Visible images of echocardiographic measurements of WT and L-cKO mice at P21d. **f** Ejection

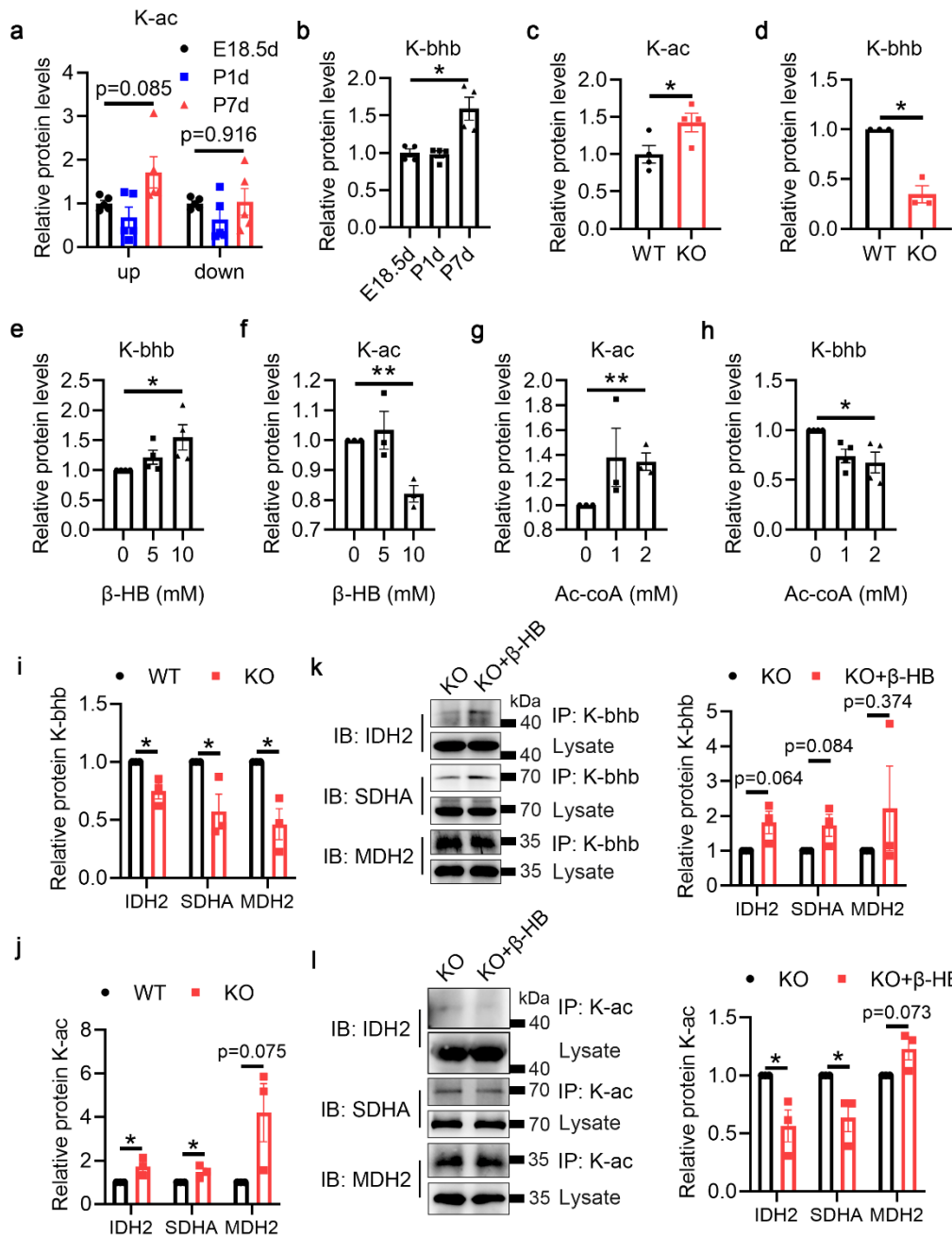
168 fractions of WT and L-cKO mice at P21d ($n = 4-5$ for each group). **g** Fractional shortening of WT and
169 L-cKO mice at P21d ($n = 4-5$ for each group). **h** Statistics of the percentages of pHH3-positive cells in
170 Fig. 6g (WT+Saline, $n = 10$; KO+Saline, $n = 8$; WT+ β -HB, $n = 5$; KO+ β -HB, $n = 8$). **i**
171 Immunofluorescence staining of BrdU and cTnT in the hearts of P5d WT and KO mice treated with
172 saline or β -HB (400 mg/kg/day though i.p. from P3d to P5d). The white arrows indicate cTnT and BrdU
173 double-positive cells. Scale bar, 20 μ m. **j** Statistics of the percentages of cTnT and BrdU double-positive
174 cells in Fig. S7i (WT+Saline, $n = 10$; KO+Saline, $n = 8$; WT+ β -HB, $n = 5$; KO+ β -HB, $n = 8$). **k** CCK-
175 8 assay of H9C2 cells treated with BSA or 200 μ M FA ($n = 8$ for each group). **l** Statistics of the
176 percentages of pHH3-positive cells in Fig. 6h ($n = 7$ for each group). **m** Statistics of the percentages of
177 PCNA-positive cells in Fig. 6h ($n = 7$ for each group). **n** CCK-8 assay of H9C2 cells treated with PBS
178 or 5 mM β -HB ($n = 8$ for each group). **o** Statistics of the percentages of pHH3-positive cells in Fig. 6i (n
179 = 5 for each group). **p** Statistics of the percentages of PCNA-positive cells in Fig. 6i ($n = 5$ for each
180 group). Data are presented as mean \pm SEM. and the P values were determined by unpaired two-tailed
181 Student's t -test. *, $P < 0.05$; **, $P < 0.01$; ***, $P < 0.001$.



182

183 **Fig. S8 Enhancing mitochondrial function inhibits cardiomyocyte cell proliferation. a**
 184 Extracellular metabolic flux analysis of the mitochondrial OCR in H9C2 cells treated with NR at different
 185 concentrations for 24h and the statistical analysis of the basal respiration and maximal respiration
 186 capacity ($n = 6$ for each group). **b** Extracellular metabolic flux analysis of the mitochondrial OCR in
 187 H9C2 cells treated with OMA at different concentrations for 24h and the statistical analysis of the basal
 188 respiration and maximal respiration capacity ($n = 5$ for each group). **c** Statistics of the percentages of

189 pHH3-positive cells in Fig. 6j ($n = 7$ for each group). **d** Immunofluorescence staining of PCNA in H9C2
190 cells treated with DMSO or NR for 24h. Scale bar, 50 μm . **e** Statistics of the percentages of PCNA-
191 positive cells in Fig. S8d ($n = 9$ for each group). **f** Immunofluorescence staining of pHH3 in H9C2 cells
192 treated with ddH₂O or OMA for 24h. Scale bar, 100 μm . **g** Statistics of the percentages of pHH3-positive
193 cells in Fig. S8f ($n = 7$ for each group). **h** Immunofluorescence staining of PCNA in H9C2 cells treated
194 with ddH₂O or OMA for 24h. Scale bar, 50 μm . **i** Statistics of the percentages of PCNA-positive cells in
195 Fig. S8h ($n = 9$ for each group). Data are presented as mean \pm SEM. and the P values were determined
196 by one-way ANOVA and unpaired two-tailed Student's t -test. *, $P < 0.05$; **, $P < 0.01$; ***, $P < 0.001$.

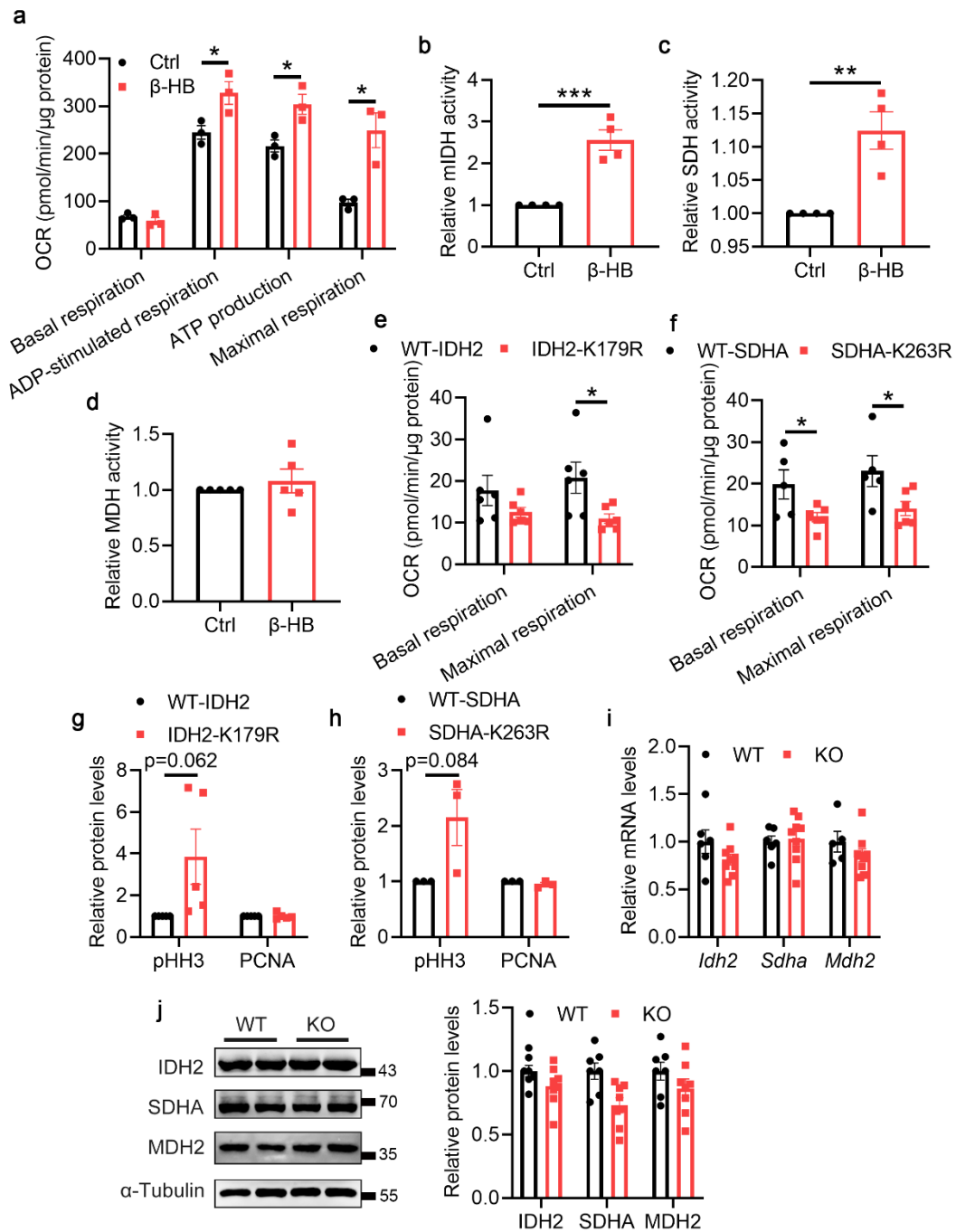


197

198 **Fig. S9 Mitochondrial protein β-hydroxybutyrylation and acetylation may account for the**
 199 **regulation of mitochondrial maturation by ketone body β-HB.** **a** Statistics of the mitochondrial
 200 protein K-ac in Fig. 7a (*n* = 5 for each group). Up: Grayscale analysis of the bands in the dashed frame
 201 in the upper part. Down: Grayscale analysis of the bands in the dashed box in the lower part. **b** Statistics
 202 of the mitochondrial protein K-bhb in Fig. 7b (*n* = 4 for each group). **c** Statistics of the mitochondrial
 203 protein K-ac in Fig. 7c (*n* = 4 for each group). **d** Statistics of the mitochondrial protein K-bhb in Fig. 7d
 204 (*n* = 3 for each group). **e** Statistics of the mitochondrial protein K-bhb in Fig. 7f (*n* = 4 for each group).
 205 **f** Statistics of the mitochondrial protein K-ac in Fig. 7f (*n* = 3 for each group). **g** Statistics of the
 206 mitochondrial protein K-ac in Fig. 7g (*n* = 3 for each group). **h** Statistics of the mitochondrial protein K-
 207 bhb in Fig. 7g (*n* = 4 for each group). **i** Statistics of the protein K-bhb of IDH2, SDHA and MDH2 in Fig.
 208 7h (*n* = 3 for each group). **j** Statistics of the protein K-ac of IDH2, SDHA and MDH2 in Fig. 7i (*n* = 3

209 for each group). **k** Immunoprecipitation assays on the hearts of KO mice at P5d treated with saline or β -
 210 HB (400 mg/kg/day though i.p. from P3d to P5d). IP: Anti-K-bhb. IB: IDH2, SDHA and MDH2. **l**
 211 Immunoprecipitation assays on the hearts of KO mice at P5d treated with saline or β -HB (400 mg/kg/day
 212 though i.p. from P3d to P5d). IP: Anti-K-ac. IB: IDH2, SDHA and MDH2. Data are presented as
 213 mean \pm SEM. and the *P* values were determined by one-way ANOVA and unpaired two-tailed Student's
 214 *t*-test. *, *P* < 0.05; **, *P* < 0.01.

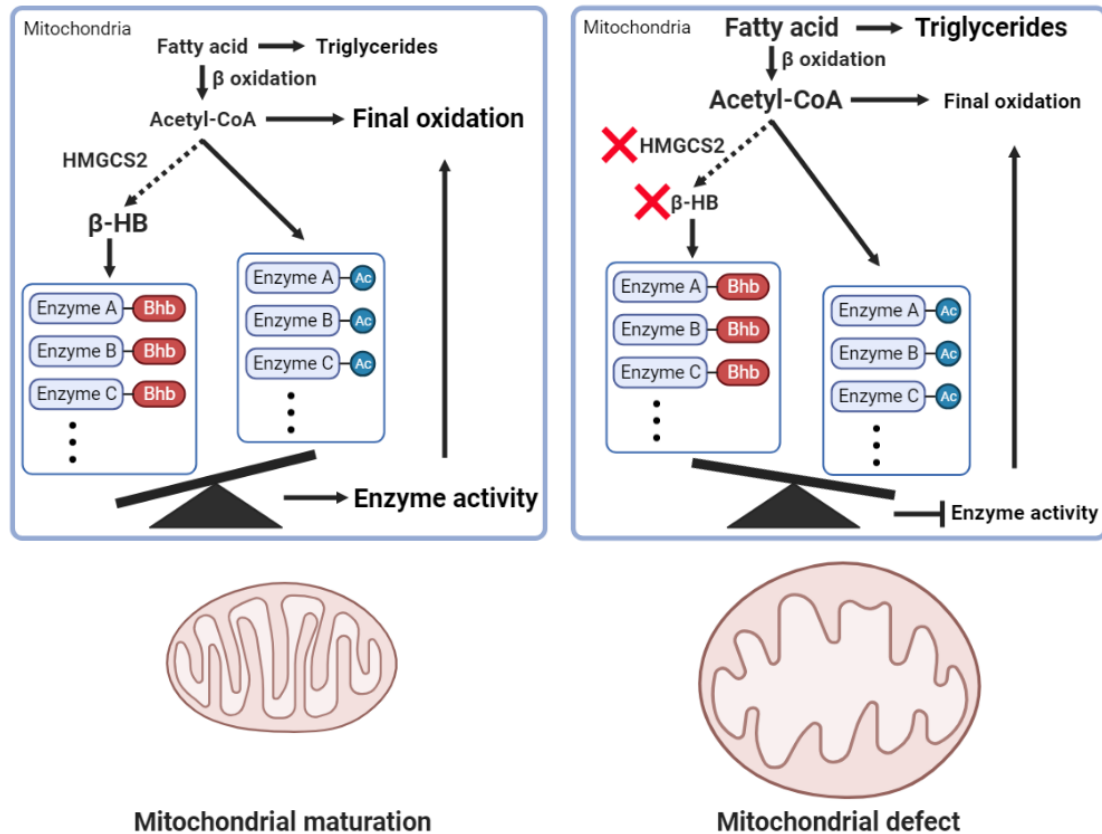
215



216

217 **Fig. S10 Ketone body β -HB promotes the enzyme activity of IDH2 and SDHA.** **a** Statistical
218 analysis of the OCR in Fig. 7m ($n = 3$ for each group). **b** Relative mitochondrial IDH (mIDH) activity of
219 293T cells treated with PBS (Control, Ctrl) or 5 mM β -HB ($n = 4$ for each group). **c** Relative SDH
220 activity of 293T cells treated with PBS or 5 mM β -HB ($n = 4$ for each group). **d** Relative MDH activity
221 of 293T cells treated with PBS or 5 mM β -HB ($n = 5$ for each group). **e** Statistical analysis of the OCR
222 in Fig. 7p ($n = 6$ for each group). **f** Statistical analysis of the OCR in Fig. 7q (WT-SDHA, $n = 5$; SDHA-
223 K263R, $n = 6$). **g-h** Statistical analysis of protein levels of pHH3 and PCNA in Fig. 7r ($n = 3-5$ for each
224 group). **i** qPCR detection of the mRNA of *Idh2*, *Sdha* and *Mdh2* in the hearts of P5d WT and KO mice
225 ($n = 5-9$). **j** Western blot detection of the protein levels of IDH2, SDHA and MDH2 in the hearts of P5d
226 WT and KO mice and the statistical analysis of the protein levels of IDH2, SDHA and MDH2 ($n = 7-8$).
227 Data are presented as mean \pm SEM. and the P values were determined by unpaired two-tailed Student's
228 t -test. *, $P < 0.05$; **, $P < 0.01$; ***, $P < 0.001$.

229



Mitochondrial maturation

Mitochondrial defect

230

231 **Fig. S11 Proposed model of ketone body regulating mitochondrial maturation in the**
 232 **postnatal heart.** The FA in the milk sucked by newborns are absorbed by cardiomyocytes and enter
 233 three metabolic pathways: mitochondrial oxidation, triglyceride synthesis, and ketogenesis. Fatty acids
 234 stimulate the expression of *Hmgcs2* in the heart. β -HB can participate in the K-bhb of metabolic enzymes
 235 (such as IDH2 and SDHA) in mitochondria, which is essential for the activity of these enzymes and
 236 mitochondrial function (left). After *Hmgcs2* is deleted, the K-bhb of metabolic enzymes in mitochondria
 237 is decreased. In addition, due to the lack of ketogenesis, acetyl-CoA is accumulated and participates in
 238 the K-ac of metabolic enzymes in mitochondria. The decrease of K-bhb and the increase of K-ac together
 239 lead to the decrease of enzyme activity and ultimately cause the abnormality of mitochondrial function
 240 (right).